Canadian Mineralogist
Vol. 21, pp. 81-91 (1983)

THE BAIE-DES-MOUTONS SYENITIC COMPLEX, LA TABATIÈRE, QUÉBEC
II. THE FERROMAGNESIAN MINERALS

ANDRÉ E. LALONDE AND ROBERT F. MARTIN
Department of Geological Sciences, McGill University, 3450 University Street, Montreal, Quebec H3A 2A7

ABSTRACT

Electron-microprobe analytical data for pyroxene, amphibole, biotite and oxides are presented for rock units of the early, intermediate and late groups of the Baie-des-Moutons syenitic complex. Pyroxenes from the pink-colored syenites of the early group are the most magnesian and, in addition, have the highest $Fe^{3+}/(Fe^{2+} + Fe^{3+})$ ratios of the complex. Biotites from the same units display the lowest $Fe/(Fe + Mg)$ ratios. Ilmenite from these rocks has a high MnO content, suggesting substitution of Mn^{2+} for Fe^{2+}. All these trends reflect a deficiency in Fe^{2+} at the magmatic stage and are interpreted as signs of magmatic oxidation. The restricted occurrence of these anomalous ferromagnesian minerals to rocks showing pink turbid feldspars suggests continuous oxidizing conditions throughout the entire paragenesis. Consequently, postmagmatic oxidation in these rocks is probably inherited from the magmatic stage. Amphiboles and oxides yield evidence of late magmatic to postmagmatic equilibration.

Keywords: syenitic complex, Baie-des-Moutons (Quebec), magmatic oxidation, pyroxene, amphibole, biotite, oxides, postmagmatic evolution.

SOMMAIRE

On présente des données analytiques, obtenues à la sonde électronique, portant sur pyroxène, amphibole, biotite et oxydes des unités lithologiques des groupes précoce, intermédiaire et tardif du complexes syénitique de Baie-des-Moutons (Québec). Les échantillons de pyroxène des syénites roses du groupe précoce accusent la plus haute teneur en magnésium; le rapport $Fe^{3+}/(Fe^{2+}+Fe^{3+})$ calculé pour ces compositions est aussi le plus élevé. De même, dans les syénites roses, la biotite possède les valeurs les plus faibles du rapport $Fe/(Fe + Mg)$. L'ilménite de ces roches montre une teneur élevée en MnO, ce qui fait supposer la substitution du Mn^{2+} au Fe^{2+}. Toutes ces caractéristiques indiquent une déficience en Fe^{2+} lors de la cristallisation du magma, que l'on interprète comme signe d'oxydation magmatique. La restriction des compositions anomales des minéraux ferromagnésiens aux roches qui possèdent un feldspath rose et turbide évoque des conditions d'oxydation continues pendant toute la paragenèse. Par conséquent, l'oxydation post-magmatique dans ces roches aurait été héritée du stade magmatique. L'amphibole et les oxydes ont été ré-équilibrés à un stade tardi-magmatique, voire post-magmatique.

Mots-clés: complexe syénitique, Baie-des-Moutons (Québec), oxydation magmatique, pyroxène, amphibole, biotite, oxydes, évolution post-magmatique.

INTRODUCTION

The evolution of the Baie-des-Moutons syenitic complex can be deduced by a very careful investigation of the constituent feldspars (volumetrically dominant) *and* the accessory ferromagnesian phases. Lalonde & Martin (1983) described how the alkali feldspar in specific cone-sheets of syenite in the Baie-des-Moutons ring-complex shows clear signs of postmagmatic recrystallization in an oxygen-rich environment. The transformed K-feldspar, intermediate microline, typically is deep pink or brown and turbid. Its color reflects the presence of very finely divided hematite, formed from iron leached upon oxidation of the adjacent ferromagnesian minerals. Because these minerals generally are less reactive than the primary monoclinic alkali feldspar, magmatic relics may survive the interaction with the interstitial fluid phase released upon crystallization of the syenitic melts. The composition of these relics, described below, suggests that the distribution of postmagmatic oxidation reflects the progressive increase in oxygen fugacity in the youngest batches of syenitic magma in an intrusive cycle. We describe here the composition of mafic minerals in order to document the different levels of oxidation at the magmatic stage and to define the intensive parameters during primary crystallization of the Baie-des-Moutons syenitic magmas.

TEXTURAL RELATIONSHIPS OF THE FERROMAGNESIAN MINERALS

Early group

Rocks of the early group (Lalonde & Martin

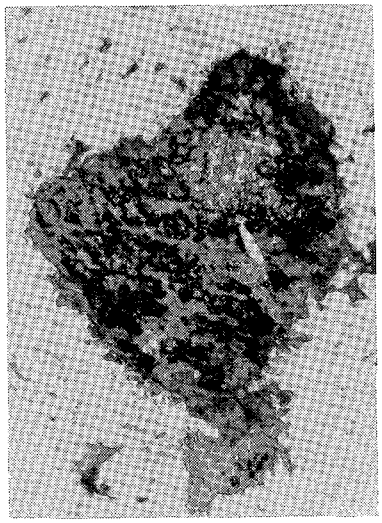

FIG. 1. Biotite and amphibole successively replacing a pyroxene core (clear). Early-group green syenites. Uncrossed polars. Field of view 3 mm.

1983) contain ferromagnesian minerals in three textural assemblages. One assemblage, typical of the green-colored units (*e.g.*, unit 1), is characterized by 1) clusters of pale green to colorless clinopyroxene, 2) breakdown of clinopyroxene to amphibole and, subsequently, to biotite, and 3) opaque minerals+apatite. These rocks are slightly richer in mafic minerals than the pink-colored units of the early group. Only one grain of orthopyroxene was found in our study of rocks of unit 1; it is broken up into numerous optically continuous islands embedded in feldspar, and thus may have been preserved metastably. Only in the pyroxene-bearing syenites of the early group is iddingsite observed, pseudomorphic after primary olivine. Amphibole grains are pleochroic brown to green and replace the clinopyroxene along crystal margins, fractures and cleavages (Fig. 1). Subsequent replacement by biotite may lead to a composite rim around a pyroxene core. Biotite also commonly rims opaque minerals.

In contrast, the pink-colored syenites of units 3, 4 and 5 contain an assemblage of highly altered pyroxene, very minor amphibole and much biotite. The aggregates of dark minerals typically consist of pyroxene (usually consumed), uralite, calcite, opaque minerals, biotite and, commonly, chlorite. Uralite and calcite seem to be major breakdown products of clinopyroxene. Biotite occurs as prominent flakes, up to 2 cm long, usually rimming altered pyroxene aggregates or opaque oxides. Amphibole grains are pleochroic brown to green, and pyroxene is pale green.

A third textural assemblage occurs in the early-group rocks of units 7 and 8. It features large, homogeneous amphibole crystals with little or no evidence of pyroxene. Ferromagnesian minerals occur in clusters with accessory phases (amphibole + opaque minerals + titanite + zircon + apatite). Amphibole grains 0.5 to 7.0 mm in length dominate these clusters. They are pleochroic green to bluish green, with bluish zones often localized along crystal margins or fracture traces. Trails of fine, aligned acicular inclusions are characteristically present in amphibole crystals from this assemblage. These small rods, ~0.004 mm in diameter and ~0.02 mm in length, which appear at high magnifications as slightly pleochroic brown material, may be the result of exsolution. These "exsolution needles" preferentially occupy the core of crystals. Similar acicular material is present in amphibole from rocks of the Almunge alkaline complex (Sweden), and is interpreted there as "droplets" of titanite (Gorbatschev 1960). Replacement of amphibole by biotite is minor. Opaque oxide minerals are rimmed by biotite or, more commonly, titanite.

Intermediate group

Two textural assemblages involving ferromagnesian minerals are recognized in the rocks of the intermediate group. Both assemblages are characterized by negligible biotite. The first textural assemblage, encountered in rocks of unit 9, is further distinguished by coarse, usually homogeneous blue-green amphibole, apparently devoid of exsolution textures. Chemical zonation is evident from the preferential development of blue pleochroism along crystal margins or transecting fractures. In some specimens, a core of chlorite and serpentine probably represents highly altered remnants of pyroxene. Most amphibole grains are free of such a core or a rim of biotite. Ferromagnesian clusters in this assemblage, 0.8 to 4.0 mm in diameter, contain amphibole, pyroxene, opaque minerals, zircon, apatite, biotite, chlorite and serpentine.

The second textural assemblage, observed in units 10 and 11, occurs in relatively more mafic rocks. It is distinguished by late crystallizing, sieve-like or macropoikilitic ferromagnesian minerals (principally amphibole, but also pyroxene and zircon). Such crystals of amphibole attain 5 cm in diameter; a single crystal may enclose hundreds of small feldspar laths (see Fig. 2 in Lalonde & Martin 1983). The amphibole crystals typically display blue-green pleo-

chroism, with deeper shades of blue developed along crystal margins and fracture traces. Pyroxene generally crystallizes before feldspar, and is engulfed along with the grains of feldspar by the late-growing amphibole crystals. The very well foliated, fine-grained units of the group show both early- and late-crystallizing pyroxene. Pyroxene crystals of both generations are deep green; in addition, the early pyroxene is zoned with deeper green crystal margins. Late sporadic hematitization of the sieve-like crystals produces large (1 to 5 cm) reddish brown spots on outcrop surfaces. Alteration to carbonates and to opaque minerals is encountered also. The former presence of primary olivine is suggested by the occurrence of iddingsite.

Late group

The sequence of crystallization is the main distinguishing factor of the ferromagnesian textural assemblage observed in the green trachytic alkali-feldspar syenites of unit 12. Pyroxene (and olivine, where present) are followed by feldspar, then by amphibole and biotite. Green syenites of unit 12 also tend to have a color index intermediate between that of the orange pink syenites (unit 13) and the associated melanocratic layers. Only in this textural assemblage (and unit) was fresh olivine observed in the complex; this observation may, however, be a sampling problem, as Davies (1968) reported olivine in four units. The olivine occurs as small subhedral phenocrysts within ferromagnesian clusters. Incipient to advanced iddingsitization was also observed in thin section. Associated pyroxene crystals are deep green, slightly pleochroic green to brown.

The orange pink trachytic alkali-feldspar syenites and associated melanocratic layers (unit 13) each display specific ferromagnesian textural assemblages. The difference between the two assemblages is essentially a reversal in the sequence of crystallization of ferromagnesian minerals. In the melanocratic layers, the main mafic minerals (pyroxene + amphibole) precede feldspar, whereas in the orange pink syenites, they crystallize after the feldspar.

In the melanocratic layers, pyroxene crystallizes first. It occurs generally as highly fractured euhedral grains, ≤ 4 mm across. These are green to deep green and slightly pleochroic. Despite numerous small crystals of amphibole and biotite closely coexisting with the pyroxene, the extent of replacement appears negligible. Amphibole is the principal ferromagnesian phase within these relatively mafic layers; it occurs as subhedral crystals 1 to 2 mm across and up to 6 mm long. These commonly show well-developed twinning. These crystals are generally pleochroic brown to green and seem homogeneous. They show little evidence of replacement of pre-existing pyroxene; only one small uralite core was observed in an amphibole crystal. Apatite and opaque minerals crystallize after pyroxene and amphibole, but before feldspar. Their distribution as roughly spherical clots that enclose the ferromagnesian minerals suggests that the silicate magma may have become saturated in oxide components, leading to an immiscible iron-oxide-rich liquid.

The orange pink trachytic syenites characteristically lack pyroxene; in addition, the ferromagnesian minerals crystallize after feldspar. Rocks from this assemblage are among the least mafic of the late group. The amphibole occurs as subhedral to anhedral crystals up to several centimetres in length. Pleochroic colors range from brown to deep green, with bluish tints commonly developed along crystal margins and cleavages. The bulk of these amphiboles is considered primary; only a few have altered cores that could have been pyroxene. Biotite occurs as large flakes closely associated with and replacing amphibole. Pleochroism is from bright fire-red to orange. Both amphibole and biotite occur along with the opaque phases and apatite as clusters up to 4 cm across, interstitial to the feldspar laths.

Mineral Chemistry

Olivine

Unfortunately, olivine is absent in the microprobe sections prepared. Davies (1968) reported a $2V_x$ value of 51° for olivine in unit 11, which would correspond, as expected, to fayalite.

Pyroxene

Pyroxene from the different units of the complex consists almost exclusively of clinopyroxene of salite to ferrosalite composition (nomenclature of Poldervaart & Hess 1951). Orthopyroxene was observed only in the green syenites of unit 1, in a single grain coexisting with clinopyroxene. Chemical compositions and structural formulae (Table 1) represent, in most cases, average results of numerous analyses performed on single grains. The proportions of Fe^{2+} and Fe^{3+} were calculated assuming stoichiometry and electrostatic neutrality. Sufficient FeO was converted to Fe_2O_3 to give a structural recalculation to 4 cations and 6 anions. The perfect stoichiometry of low-pressure igneous pyroxene has been demonstrated by Cawthorn & Collerson (1974). Electron-microprobe tra-

TABLE 1. COMPOSITIONS AND STRUCTURAL FORMULAE OF PYROXENES FROM UNITS 1, 5, 11 AND 12

Rock unit	11	11	12	12	12	12	5	5	1	1	1	1	1	1
Specimen	P8655		P8657				78-78A2		78-63					
Grain number	2	4	1	2	4	5	1	5	1	2	3	4	5	6
SiO_2	51.52	51.15	50.74	50.52	51.36	50.95	53.02	51.12	51.07	50.82	50.59	51.16	50.70	51.06
TiO_2	0.40	0.43	0.30	0.33	0.53	0.40	0.61	0.63	0.54		0.30	0.23	0.27	0.27
Al_2O_3	0.78	0.72	0.69	0.83	0.93	0.67	1.06	1.04	1.21	0.20	0.89	0.35	0.52	0.66
Fe_2O_3	4.95	5.19	3.72	5.01	4.32	3.92	3.49	2.80	3.27	4.03	1.77	1.94	1.69	1.70
Cr_2O_3	0.04	0.21	0.09	0.09	0.01	0.08	0.09	0.20	0.19		0.02	0.09	0.11	0.01
FeO	15.52	14.93	17.53	17.37	16.13	16.68	8.25	7.57	13.35	17.23	17.28	14.88	17.03	16.49
MnO	1.27	1.23	1.22	1.36	1.27	1.28	1.15	1.19	0.99	1.41	0.90	0.94	0.84	0.98
MgO	6.49	6.17	5.64	5.04	6.38	5.82	11.07	11.35	9.69	6.19	7.39	8.56	7.46	8.11
CaO	20.04	20.26	21.03	21.12	20.92	21.38	22.22	20.80	20.65	21.78	21.17	21.87	21.57	21.55
Na_2O	1.69	1.81	1.10	1.27	1.31	1.19	1.34	1.22	0.74	0.68	0.47	0.49	0.44	0.36
K_2O	0.04	0.01	0.03	0.01	0.07	0.01	0.05	0.13	0.02		0.03			0.02
Total	102.74	102.11	102.09	102.95	103.23	102.38	102.35	98.05	101.72	102.34	100.81	100.51	100.63	101.21
FeO*	19.97	19.60	20.88	21.88	20.02	20.21	11.39	10.09	16.29	20.86	18.87	16.63	18.55	18.02
Structural formulae based on 4 cations and 6 anions														
Si	1.962	1.961	1.962	1.945	1.952	1.960	1.959	1.963	1.936	1.963	1.963	1.974	1.971	1.967
Al^{iv}	0.035	0.033	0.031	0.038	0.042	0.030	0.041	0.037	0.054	0.009	0.037	0.016	0.024	0.030
Ti	0.003	0.006	0.007	0.010	0.006	0.010			0.010			0.007	0.005	0.003
Fe^{3+}				0.007						0.028		0.003		
Al^{vi}							0.005	0.010			0.004			
Ti	0.009	0.006	0.002		0.009	0.002	0.017	0.018	0.005		0.009		0.003	0.005
Fe^{3+}	0.142	0.150	0.108	0.138	0.124	0.113	0.097	0.081	0.093	0.089	0.052	0.053	0.049	0.049
Fe^{2+}	0.494	0.479	0.567	0.559	0.513	0.537	0.255	0.243	0.423	0.556	0.561	0.480	0.554	0.531
Mn	0.041	0.040	0.040	0.044	0.041	0.042	0.036	0.039	0.032	0.046	0.030	0.031	0.028	0.032
Cr	0.001	0.006	0.003	0.003		0.002	0.003	0.006	0.006		0.001	0.003	0.003	
Mg	0.368	0.352	0.325	0.289	0.361	0.334	0.610	0.650	0.547	0.356	0.427	0.492	0.432	0.466
Ca	0.818	0.832	0.871	0.871	0.852	0.881	0.880	0.856	0.839	0.901	0.880	0.904	0.898	0.889
Na	0.125	0.135	0.082	0.095	0.097	0.089	0.096	0.091	0.054	0.051	0.035	0.037	0.033	0.027
K	0.002		0.001		0.003		0.002	0.006	0.001		0.001			0.001
Ionic proportions														
Fe/(Fe+Mg)	0.633	0.641	0.675	0.707	0.638	0.661	0.366	0.333	0.485	0.644	0.589	0.520	0.583	0.554
$Fe^{3+}/(Fe^{2+}+Fe^{3+})$	0.223	0.238	0.160	0.206	0.195	0.174	0.276	0.250	0.180	0.174	0.085	0.104	0.081	0.084

*Total Fe calculated as FeO.

verses confirm the homogeneous nature of these pyroxenes; only in a few cases was zoning suggested by slight increases in the ratio Fe/(Fe + Mg) from core to rim.

In the compositional plane En–Fs–Wo (Fig. 2), pyroxenes evolve toward progressively more iron-rich members in the sequence early group → late group. Indeed, in general, Fe/(Fe + Mg) ratios range from 0.56 in the oldest rocks of the complex (green syenites) to 0.67 in the youngest pyroxenes analyzed (unit 12). However, a marked reversal in this evolutionary trend occurs in the pyroxene of the pink syenites in the early group (units 3 & 5). With an Fe/(Fe + Mg) ratio of 0.35, pyroxene from units 3 and 5 is clearly the most magnesian of the intrusion; yet these units fail to display the usual features of magmatically more primitive rocks (*e.g.*, calcic plagioclase, high color index). Similar departures from the expected Fe-enrichment trend have been reported in pyroxenes from the Finnmarka (Czamanske & Wones 1973) and Ben Nevis complexes (Haslam 1968). In both cases, highly oxidizing conditions are believed responsible for the incorporation of iron dominantly as Fe^{3+} in oxide phases, thereby leading to a deficiency in Fe^{2+} in the magma at the time the pyroxene nucleated and grew. Consequently, Mg substitutes for ferrous iron in pyroxene. Besides the Fe/(Fe + Mg) ratios, oxidation in the magma is suggested by the $Fe^{3+}/(Fe^{2+} + Fe^{3+})$ ratio inferred for the pyroxene (Fig. 3): that from units 3 and 5 shows the highest proportion of ferric iron. Additional evidence for oxidation at the magmatic stage is presented below.

The analyzed crystals of pyroxene fail to define a consistently increasing trend towards $NaFe^{3+}Si_2O_6$, as observed in numerous alkaline complexes (Tyler & King 1967, Nash & Wilkinson 1970, Larsen 1976, Neumann 1976, Mitchell & Platt 1978). The most sodic pyroxene, containing approximately 15 mole % Ac, comes from the grey syenites of the intermediate group (unit 11). Note that the feldspar mineralogy of the intermediate group syenites was considered typical of that from peralkaline rocks (Lalonde & Martin 1983).

Amphibole

Amphibole crystals from representative specimens of all three intrusive groups of the complex

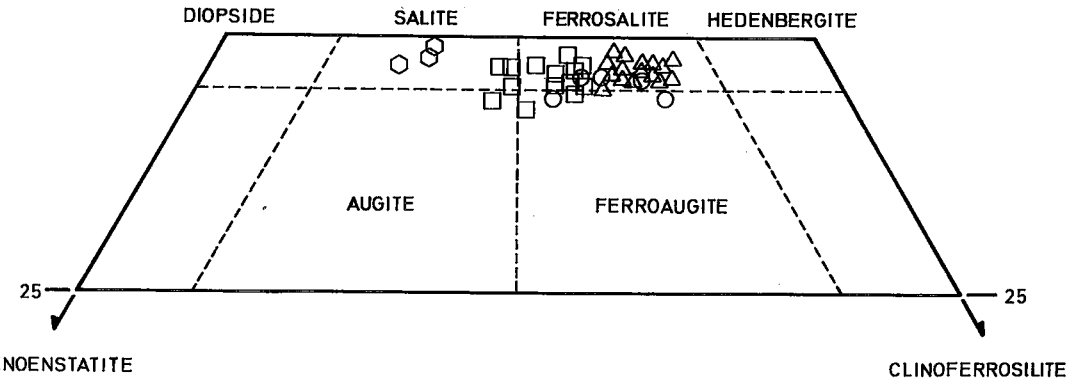

FIG. 2. Pyroxene compositions represented in the compositional plane En–Fs–Wo. Nomenclature is that proposed by Poldervaart & Hess (1951). Squares represent early-group green units, hexagons, early-group pink units, circles, intermediate-group grey units, and triangles, late-group units.

were analyzed by electron microprobe. Data are presented for 1) the green syenites of unit 1, 2) the grey syenites of unit 11 and 3) both green and orange pink syenites of units 12 and 13. In most cases, compositions and structural formulae (Table 2) represent averages of several analyses performed on single grains. Nomenclature and mineral-recalculation procedures follow the recommendations of Leake (1978). However, in the cases where Si, Al and Cr do not total 8.00 in the *T* site, the necessary Fe^{2+} was converted to Fe^{3+} rather than assign Ti to the tetrahedral position. Since the amount of Fe^{3+} thus calculated may not represent the actual Fe^{3+} contents, it was not expressed in weight % Fe_2O_3 in Table 2. Amphibole compositions encountered include ferro-edenitic hornblende, ferro-edenite and ferro-richterite, all of which have complete *A*-site occupancies (or nearly so). Many of these amphibole grains can further be characterized by the prefixes titanian, potassian, or both.

Unlike their pyroxene counterparts, amphibole compositions show a relatively small range of values of the Fe/(Fe + Mg) ratio. These vary from 0.691 to 0.826 without apparent relationship to age or color of units. The major compositional differences are expressed in the sodium and aluminum contents. Amphibole crystals from the early and late groups are relatively homogeneous and calcic, and plot in the ferro-edenite to ferro-edenitic hornblende fields (Fig. 4). Amphiboles of the intermediate group show considerably more compositional variation; they are calcic to sodic–calcic and evolve with increasing Si and Na in the *M*4 site from ferro-edenite to ferro-richterite (Fig. 5). The most sodic compositions (Na_A 0.63, Na_{M4} 0.77) are

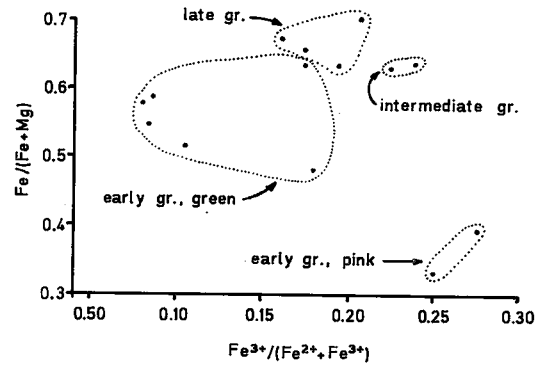

FIG. 3. Variations, in pyroxenes, of the Fe/(Fe+Mg) ratio as a function of the oxidation state of iron [$Fe^{3+}/(Fe^{2+}+Fe^{3+})$].

samples of the pleochroic-blue zones developed near crystal margins and along cleavages. Intermediate-group amphiboles are, in addition, characterized by lower aluminum contents (average wt. % Al_2O_3 is 2.95 for intermediate-group amphibole, 6.15 for amphibole from other groups). Such features may reflect a lower pressure of crystallization for rocks of the intermediate group; aluminum content in amphibole has been demonstrated to increase with increasing pressure of crystallization (Leake 1965). Titanium and potassium increase gradually with decreasing age of the enclosing rocks.

Biotite

Results of analyses of biotite from green syenites (unit 1) and pink syenites of the early group (unit 3 and 5) and both green and orange pink syenites of the late group (unit 12 and 13,

TABLE 2. COMPOSITIONS AND STRUCTURAL FORMULAE OF AMPHIBOLES FROM UNITS 1, 11, 12 AND 13

Rock unit		11	11	11	11	12	12	12	12	13	13	1
Specimen		P8655				P8657				77-2283		78-63
Grain number		1	2	3	4	2	3	4	5	1	2	2
SiO_2		48.75	48.04	48.85	47.57	43.55	44.69	44.59	43.88	42.43	42.98	45.74
TiO_2		1.34	2.09	1.02	1.71	2.58	2.52	2.48	2.49	2.29	2.27	1.29
Al_2O_3		2.36	3.86	2.39	3.17	6.40	6.46	5.89	5.74	6.74	6.83	4.98
Cr_2O_3		0.18	0.09	0.04	0.03	0.07	0.05	0.09	0.03	0.00	0.08	0.00
FeO*		30.67	25.58	30.19	27.61	26.38	26.34	27.68	27.01	28.38	26.72	27.86
MnO		1.40	1.11	1.31	1.22	1.06	1.18	0.87	1.04	2.04	1.40	1.14
MgO		3.89	6.42	4.20	5.27	5.27	5.73	4.98	4.18	3.36	4.86	5.96
CaO		6.14	8.08	6.10	7.48	9.60	9.87	9.03	9.09	8.98	9.21	10.02
Na_2O		4.67	4.18	4.37	4.25	3.37	3.44	3.58	3.29	3.59	3.51	1.99
K_2O		1.28	1.34	1.24	1.24	1.48	1.38	1.53	1.40	1.42	1.53	0.54
Total		100.68	100.79	99.68	99.56	99.76	101.64	100.71	98.16	99.22	99.86	99.54
Structural formulae based on 23 oxygens: $A_{0-1}B_2C_5T_8O_{23}$												
Si		7.553	7.288	7.609	7.380	6.782	6.808	6.891	6.950	6.746	6.747	7.089
Al^{iv}	*T*	0.431	0.689	0.391	0.579	1.175	1.159	1.072	1.050	1.254	1.253	0.910
Cr		0.016	0.011		0.003	0.009	0.006	0.011				0.001
Fe^{3+}			0.012		0.038	0.034	0.027	0.026				
Al^{vi}				0.048					0.022	0.007	0.009	
Cr		0.005		0.005					0.003		0.009	
Ti	*C*	0.156	0.239	0.119	0.200	0.302	0.289	0.287	0.296	0.272	0.267	0.149
Mg		0.897	1.451	0.975	1.218	1.221	1.299	1.145	0.987	0.794	1.134	1.377
Fe^{2+}		3.942	3.234	3.853	3.545	3.401	3.327	3.549	3.577	3.774	3.508	3.474
Mn			0.076		0.037	0.076	0.085	0.019	0.115	0.153	0.073	
Fe^{2+}		0.031		0.080								0.136
Mn		0.183	0.067	0.172	0.123	0.064	0.066	0.094	0.024	0.121	0.113	0.149
Ca	*B*	1.016	1.312	1.018	1.243	1.601	1.609	1.494	1.542	1.529	1.549	1.664
Na		0.770	0.621	0.730	0.634	0.335	0.325	0.412	0.434	0.350	0.338	0.051
Na	*A*	0.632	0.609	0.589	0.644	0.683	0.690	0.659	0.577	0.756	0.729	0.546
K		0.247	0.260	0.246	0.246	0.295	0.268	0.301	0.281	0.288	0.305	0.106

* Total Fe calculated as FeO. Fe^{3+} was converted from Fe^{2+} to fill *T*-sites. Since the amount of Fe^{3+} thus calculated does not represent actual Fe^{3+} contents, it was not expressed in weight % Fe_2O_3 above.

respectively) are presented in Table 3. No data are provided for the intermediate group, as biotite is virtually absent from these rocks. Results quoted in Table 3 are averages of electron-microprobe analyses performed on numerous grains from individual sections. In terms of the phlogopite–annite–eastonite–siderophyllite diagram (Fig. 6), biotite compositions from the complex display a bimodal distribution of Fe/(Fe + Mg) ratios. Pink syenites from the early group contain magnesium-rich biotite [Fe/(Fe + Mg) ratios from 0.44 to 0.49]. The biotite from early-group green, late-group green and orange pink syenites displays a much higher ratio (0.71 to 0.83), plotting near the annite corner. As with the pyroxenes, this unexpected compositional "reversal" is ascribed to oxidizing magmatic conditions that resulted in a deficiency in Fe^{2+} during the crystallization of the early-group pink syenites. Once again, similar trends, also attributed to magmatic oxidation, are observed in biotite of the Kolyvan (Potap'yev 1964), Ben Nevis (Haslam 1968), Finnmarka (Czamanske & Wones 1973) and Klokken complexes (Parsons 1979). In general, zoning is absent except for titanium, which usually increases dramatically toward biotite–ilmenite grain boundaries. This may indicate that the outer part of some biotite flakes grew at a late stage, at the expense of the ilmenite grains.

Oxide minerals

Only one magnetite–ilmenite pair (specimen 78–78A2, unit 5) was analyzed; the results, calculated according to the method outlined by Carmichael (1967), give compositions of Hem_6Ilm_{94} for the ilmenite and $Mt_{97}Uv_3$ for the magnetite. Temperature–$f(O_2)$ implications are discussed below. MnO contents appear significantly higher in ilmenite from early-group pink syenites than in corresponding green syenites (5.81 *versus* 1.12 wt. % MnO). This observation may very well be another reflection of oxidizing conditions in the magma that gave the pink syenites. Czamanske & Mihalik (1972) also documented an enrichment in manganese in ilmenite from the Finnmarka complex; they interpreted this as a consequence of the Fe^{2+} deficiency in the highly oxidized granitic magmas at the stage of crystallization of ilmenite.

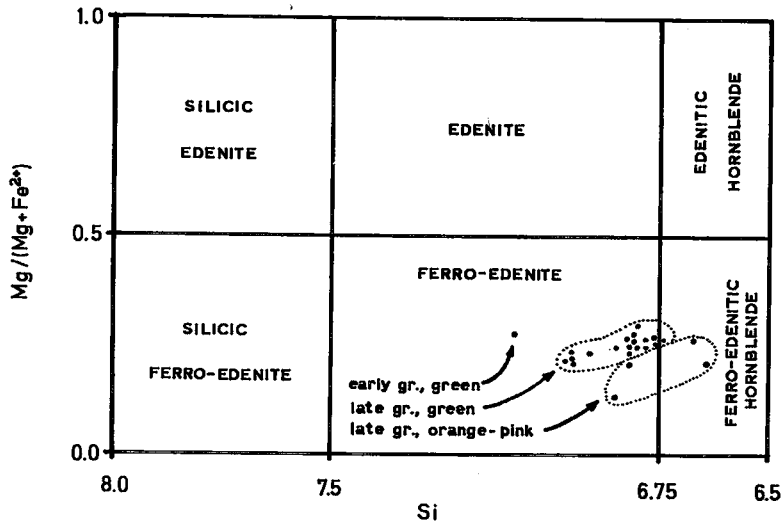

FIG. 4. Chemical evolution of calcic amphiboles of the early and late groups in terms of Leake's classification (1978) for calcic amphiboles, where: 1) $(Ca+Na)_B \geqq 1.34$, 2) $Na_B < 0.67$ and $(Na+K)_A \geqq 0.50$, $Ti < 0.50$, $Fe^{3+} \leqq {}^{vi}Al$ or $Fe^{3+} > {}^{vi}Al$.

EVALUATION OF INTENSIVE PARAMETERS

Equilibria among the mineral phases in a rock can provide a valuable insight into the range of T, P, $P(H_2O)$ and $P(O_2)$ conditions that prevailed at the time of crystallization. Recent work on phase equilibria involving richterite and ferro-richterite (Charles 1975, 1977) gives maximum thermal stability limits for intermediate-group amphiboles. The distribution of Fe and Ti between coexisting magnetite and ilmenite, investigated by Buddington & Lindsley (1964), has long been used as a geothermometer and oxygen geobarometer. More recently documented is the use of Mg and Fe^{2+} distribution between ilmenite and clinopyroxene as a geothermometer (Bishop 1980). Note that the general absence of orthopyroxene and fresh olivine precludes the application of a number of potentially useful geothermometers.

Amphibole stability

Maximum thermal stability of intermediate compositions along the richterite–ferro-richterite join $Na_2CaMg_5Si_8O_{22}(OH)_2$ – $Na_2CaFe_5Si_8O_{22}(OH)_2$ are known at total pressures of 1 kbar for various oxygen buffers (Charles 1977). In the case of the ferro-richterite from the intermediate group (sample P8655), crystallization probably proceeded at or near the QFM buffer since iddingsite (as a pseudomorph of olivine), iron oxide and quartz (in some cases) coexist in these rocks. A member of the richterite – ferro-richterite series with a composition $Na_2CaMgFe_4Si_8O_{22}(OH)_2$ has a maximum stability of 730 ± 10°C at the QFM buffer. Increasing $f(O_2)$ to the hematite–magnetite buffer drastically decreases the upper stability limit of such an amphibole to 550 ± 20°C.

Fe–Ti–oxide geothermometry

The single ilmenite–magnetite pair (compositions Hem_6Ilm_{94} and $Mt_{97}Uv_3$) suggests $f(O_2)$–T conditions beyond the field of calibration of Buddington & Lindsley (1964). By extrapolation, a temperature of 400°C and an oxygen fugacity of 10^{-25} atm can be inferred. Even though based upon a large extrapolation, these conditions are reasonable for postmagmatic recrystallization, a process well known to disrupt the primary chemistry of Fe–Ti oxides. At temperatures of 400°C, an oxygen fugacity of 10^{-25} atm is relatively high, near the HM buffer (Lindsley 1976, Fig. L–20), as expected from the occurrence of postmagmatic hematite in the turbid feldspar. The high MnO content of ilmenite from the pink syenites definitely contributes an important uncertainty to this estimate.

The ilmenite–clinopyroxene geothermometer of (Bishop (1980) was applied to early-group green and pink syenites and to late-group green syenites. In all cases, temperatures obtained are

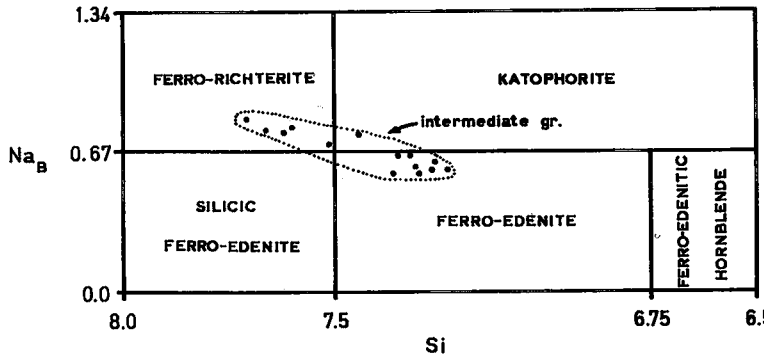

FIG. 5. Chemical evolution of calcic and sodic–calcic amphiboles of the intermediate group in terms of Leake's classification (1978) for calcic and sodic–calcic amphiboles, where: 1) $(Ca+Na)_B \geqslant 1.34$, 2) $(Na+K)_A \geqslant 0.50$, and 3) $0 \leqslant Mg/(Mg+Fe^{2+}) < 0.50$.

subsolidus, below the calibrated range of this geothermometer. However, this geothermometer commonly gives unrealistically low temperatures of magmatic crystallization, as found by d'Arco & Maury (1981) in a study of comparative geothermometry.

DISCUSSION

Much of the evidence presented here indicates that strongly oxidizing conditions prevailed during the formation of pinkish syenites from the early group and, to a lesser extent, from the late group. In the case of the early-group rocks, this evidence includes Mg-enriched pyroxene and biotite, feldspar strikingly reddened with hematite, and Mn-enrichment in ilmenite. As pyroxene commonly retains its primary composition in metaigneous rocks, it probably reflects magmatic conditions in these rocks. Biotite in these rocks certainly originated, in part, by replacement of pyroxene, and its Mg-rich nature may be inherited from these minerals. However, manganese enrichment in late (if not postmagmatic) ilmenite, a consequence of Fe^{2+} depletion, suggests the persistence of oxidizing conditions at the postmagmatic stage. Finally, turbid red feldspars also reflect oxidation, but at a much later stage, in the field of stability of microcline, as demonstrated by Lalonde & Martin (1983). We conclude that in the pink syenites of the early group, oxidation effects persisted throughout the sequence of crystallization, from early magmatic to late postmagmatic. On the other hand, late-group orange pink syenites show no evidence of magmatic oxidation in their ferromagnesian mineral chemistry; only minor postmagmatic oxidation occurred in these rocks, as implied by their moderately turbid alkali feldspars.

Numerous causes can be invoked to account for the increase in $f(O_2)$ at Baie-des-Moutons, but water buildup accompanying crystal fractionation in the magma seems the most plausible. In order to act as an oxidant, water must first be exsolved, then dissociate into H_2 and O_2; a net loss H_2 must then occur to the surrounding walls (Czamanske & Wones 1973). In such a situation, oxidation will be initiated upon H_2O saturation in the melt. As oxidation effects are observed in early-crystallizing minerals (*e.g.*, pyroxene from the early-group pink syenites), magmas that gave rise to these rocks must have had a relatively high initial water content, and thus attained saturation soon after crystallization began. The sudden and early vesiculation of these water-rich melts may well have contributed to open new fissures or to enlarge pre-existing fractures through which the magmas could have become contaminated with atmospheric oxygen to further increase their level of oxidation (Haslam 1968). The preservation of oxidizing fluids in their respective cone-sheets, probably a function of low host-rock permeability, would have ensured the continuation of oxidation trends to the postmagmatic stage. It follows that vesiculation-induced oxidation is a feature of magmas emplaced at shallow depths. We recall here that the water responsible for the sequence of postmagmatic changes is of magmatic derivation, as indicated by the oxygen-isotope geochemistry of the disturbed rocks (Lalonde & Martin 1983).

Ferromagnesian phases in the intermediate

TABLE 3. COMPOSITIONS AND STRUCTURAL FORMULAE OF BIOTITES IN UNITS 1, 3, 5, 12 AND 13

Rock unit	12	12	13	13	5	5	5	1	1	1	1	1	1	3
Specimen		P8657		77-2283		78-78A2					78-63			78-23
Grain number		5	1	2	2	4	6	1	2	3	4	5	6	2
SiO_2	36.50	36.22	35.55	36.81	39.22	38.68	38.44	35.70	34.73	35.00	34.89	35.03	34.52	39.33
TiO_2	4.18	3.84	3.63	2.89	4.22	4.76	4.50	4.58	5.09	5.29	5.34	5.28	5.23	2.83
Al_2O_3	10.33	10.53	9.99	10.12	11.70	11.75	11.74	12.28	12.06	11.86	12.01	11.79	11.83	10.61
Cr_2O_3		0.08	0.06	0.09	0.06	0.02	0.04		0.10	0.03		0.01		0.02
FeO*	32.67	33.13	33.77	31.50	18.81	20.55	20.17	28.04	29.52	29.08	28.83	28.55	29.13	19.47
MnO	0.49	0.47	1.44	1.31	0.58	0.60	0.45	0.31	0.27	0.24	0.30	0.41	0.37	0.41
MgO	3.77	4.42	3.37	5.93	12.94	12.06	12.17	6.45	4.78	5.73	5.37	5.73	5.34	13.14
CaO				0.02				0.04			0.01	0.02	0.09	
Na_2O	0.16	0.58	0.52	0.61	0.49	0.49	0.59	0.28	0.30	0.22	0.12	0.30	0.24	0.29
K_2O	8.96	9.41	9.15	9.27	10.18	9.88	10.03	9.44	9.39	9.15	8.84	9.16	9.07	10.00
TOTAL	97.07	98.68	97.48	98.55	98.20	98.79	98.13	97.12	96.24	96.60	95.70	96.28	95.82	96.10
Structural formulae based on 22 oxygens														
Si	5.871	5.766	5.806	5.835	5.829	5.759	5.760	5.623	5.582	5.577	5.589	5.593	5.561	5.985
^{IV}Al	1.959	1.976	1.923	1.891	2.050	2.062	2.074	2.280	2.285	2.228	2.273	2.219	2.247	1.903
^{IV}Ti	0.171	0.258	0.271	0.274	0.121	0.179	0.166	0.097	0.133	0.195	0.138	0.188	0.192	0.112
^{VI}Ti	0.335	0.202	0.142	0.071	0.351	0.354	0.341	0.446	0.482	0.439	0.507	0.446	0.442	0.212
Fe	4.395	4.411	4.612	4.176	2.338	2.559	2.528	3.694	3.968	3.875	3.871	3.813	3.924	2.478
Mn	0.067	0.063	0.199	0.176	0.073	0.076	0.057	0.041	0.037	0.032	0.041	0.055	0.050	0.053
Cr		0.010	0.008	0.011	0.007	0.002	0.005		0.013	0.004		0.001		0.002
Mg	0.904	1.049	0.820	1.401	2.866	2.676	2.718	1.514	1.145	1.361	1.285	1.364	1.282	2.980
Ca				0.003				0.007			0.002	0.003	0.016	
Na	0.050	0.179	0.165	0.187	0.141	0.141	0.171	0.086	0.093	0.068	0.037	0.093	0.075	0.086
K	1.839	1.911	1.906	1.875	1.930	1.877	1.918	1.897	1.925	1.860	1.811	1.866	1.864	1.941
Fe/(Fe+Mg)	0.829	0.809	0.850	0.749	0.449	0.489	0.482	0.709	0.776	0.741	0.751	0.737	0.754	0.454

*Total Fe calculated as Feo.

group display a pattern of enrichment in Na distinct from other rocks of the complex. The parental liquid for this group was most likely Na-enriched, as is evident from the relatively sodic composition of the primary pyroxene. Sodium buildup with increasing fractionation is also reflected in the amphibole, which defines a clear trend from ferro-edenite to ferro-richterite. This buildup then culminates at the postmagmatic stage with crystallization of deuteric albite, giving the sawtooth margins around perthite phenocrysts, and with the growth of blue amphiboles along the grain boundaries and cleavages of the primary amphibole; both phenomena presumably reflect the presence of a sodium-rich vapor phase. The abundance of calcite as an alteration mineral (after either pyroxene or amphibole) and as a late accessory phase supports an active role of CO_2 in this vapor phase. This sodium-rich mixed volatile phase, evidently mildly alkaline in composition, could also very efficiently catalyze the Al/Si ordering reaction in the alkali feldspars. However, on account of its significant CO_2 content, and consequently lower $P(H_2O)$ and $f(O_2)$, it would not necessarily promote postmagmatic oxidation to the extent seen in other groups of the complex.

The macropoikilitic amphibole phenocrysts observed in certain intermediate-group units

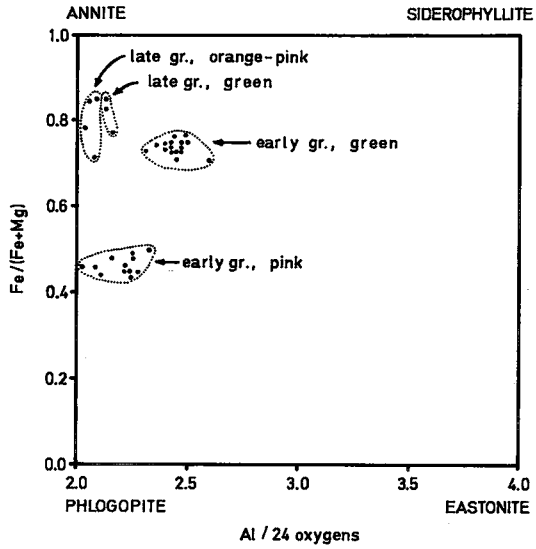

FIG. 6. Compositional variations of biotite expressed in the phlogopite–annite–eastonite–siderophyllite compositional field.

represent not only late growth of few nuclei (on account of a low thermal stability limit), but also rapid growth (as suggested by their crystal morphology), promoted by crystallization from highly evolved, gas-charged interstitial residual

melts. Such textural evidence of late and rapid crystal growth are commonly observed in sodic amphiboles in anorogenic complexes (Taylor 1979).

Late-crystallizing ferromagnesian minerals are also a characteristic feature of rocks of the late group. Unlike their counterparts of the intermediate group, ferromagnesian minerals of the late group show no evidence of rapid growth such as macropoikilitic rosettes. Both pyroxene and amphibole display much less sodic compositions than in the intermediate group. The magmatic layering observed in the trachytic-textured rocks of the late group is associated with reversals in the sequence of appearance of the dominant minerals. In the orange pink syenites of unit 13, amphibole and biotite crystallized after the feldspar. However, in the melanocratic layers of this unit, pyroxene and amphibole crystallized before the feldspar. Detailed textural studies were not done on these mafic layers; whether these crystallized before or after the associated orange pink syenites is unknown.

The trachytic texture of the late group suggests its emplacement as a viscous crystal mush. Such a viscous medium would most likely inhibit the floating and sinking of crystals due to density differences. In addition, the irregular morphology and reversals in paragenetic sequence of ferromagnesian phases both preclude a straightforward cumulate origin for the melanocratic layers. As an alternate mechanism of segregation, we suggest that a relatively mafic liquid accumulated at the crystal–melt interface, mainly as a function of poor ionic diffusion in the viscous magmas as feldspar crystallization proceeded from the walls inward. Once sufficient mafic liquid had accumulated, ferromagnesian minerals would have become liquidus phases, crystallizing a mafic layer and thereby consuming the mafic liquid. Disruption of the melanocratic layers would be a function of movements in the hot mushes of crystal + melt(s). Repetitive "inversed" mineral layering has also been described for the Klokken gabbro-syenite complex in Greenland (Parsons 1979). In this case, the layering was attributed to undercooling of a magma submitted to rhythmic fluctuations in pressure, as expected in a subvolcanic environment.

Interestingly, as enrichment in mafic constituents progresses to form these melanocratic layers, opaque oxides and apatite together begin to act as a matrix to the ferromagnesian minerals, suggesting the occurrence of a late-crystallizing oxide–phosphate liquid. This observation may be consistent with suggestions of an immiscibility relationship between a melt that crystallizes to iron oxide + apatite and a very iron-rich silicate melt (Philpotts 1967).

Acknowledgements

We thank Mr. D. Kempson and Professor P. L. Roeder of the Department of Geological Sciences, Queen's University for their assistance and hospitality in connection with the analytical work. We also thank two anonymous referees selected by Associate Editor L. T. Trembath. Research expenses were covered by a Natural Sciences and Engineering Research Council grant (A7721) to R.F. Martin.

References

Bishop, F.C. (1980): The distribution of Fe^{2+} and Mg between coexisting ilmenite and pyroxene with applications to geothermometry. *Amer. J. Sci.* **280**, 46-77.

Buddington, A.F. & Lindsley, D.H. (1964): Iron–titanium oxide minerals and synthetic equivalents. *J. Petrology* **5**, 310-357.

Carmichael, I.S.E. (1967): The iron-titanium oxides of salic volcanic rocks and their associated ferromagnesian silicates. *Contr. Mineral. Petrology* **14**, 36-64.

Cawthorn, R.G. & Collerson, K.D. (1974): The recalculation of pyroxene end-member parameters and the estimation of ferrous and ferric iron content from electron microprobe analyses. *Amer. Mineral.* **59**, 1203-1208.

Charles, R.W. (1975): The phase equilibria of richterite and ferrorichterite. *Amer. Mineral.* **60**, 367-374.

——— (1977): The phase equilibria of the intermediate composition on the pseudobinary $Na_2CaMg_5Si_8O_{22}(OH)_2$ – $Na_2CaFe_5Si_8O_{22}(OH)_2$. *Amer. J. Sci.* **277**, 594-625.

Czamanske, G.K. & Mihalik, P. (1972): Oxidation during magmatic differentiation, Finnmarka complex, Oslo area, Norway. 1. The opaque oxides. *J. Petrology* **13**, 493-509.

——— & Wones, D.R. (1973): Oxidation during magmatic differentiation, Finnmarka complex, Oslo area, Norway. 2. The mafic silicates. *J. Petrology* **14**, 349-380.

d'Arco, P. & Maury, R.C. (1981): Comparative geothermometry of some magnetite–ilmenite–orthopyroxene–clinopyroxene associations from volcanic rocks. *Can. Mineral.* **19**, 461-467.

DAVIES, R. (1968): *Geology of the Mutton Bay Intrusion and Surrounding Area, North Shore, Gulf of St. Lawrence, Quebec.* Ph.D. thesis, McGill Univ., Montreal, Que.

GORBATSCHEV, R. (1960): On the alkali rocks of Almunge. A preliminary report on a new survey. *Geol. Inst. Univ. Uppsala Bull.* **39**, 1-69.

HASLAM, H.W. (1968): The crystallization of intermediate and acid magmas at Ben Nevis, Scotland. *J. Petrology* **9**, 84-104.

LALONDE, A.E. & MARTIN, R.F. (1983): The Baie-des-Moutons syenitic complex, La Tabatière, Québec. I. Petrography and feldspar mineralogy. *Can. Mineral.* **21**, 65-79.

LARSEN, L.M. (1976): Clinopyroxenes and coexisting mafic minerals from the alkaline Ilimaussaq intrusion, south Greenland. *J. Petrology* **17**, 258-290.

LEAKE, B.E. (1965): The relationship between tetrahedral aluminum and the maximum possible octahedral aluminum in natural calciferous and subcalciferous amphiboles. *Amer. Mineral.* **50**, 843-851.

——— (1978): Nomenclature of amphiboles. *Can. Mineral.* **16**, 501-520.

LINDSLEY, D.H. (1976): Experimental studies on oxide minerals. *In* Oxide Minerals (D. Rumble III, ed.) *Mineral. Soc. Amer. Short Course Notes* **3**, L61-88.

MITCHELL, R.H. & PLATT, R.G. (1978): Mafic mineralogy of ferroaugite syenite from the Coldwell alkaline complex, Ontario, Canada. *J. Petrology*, **19**, 627-652.

NASH, W.P. & WILKINSON, J.F.G. (1970): Shonkin Sag laccolith, Montana. 1. Mafic minerals and estimates of temperature, pressure, oxygen fugacity and silica activity. *Contr. Mineral. Petrology* **25**, 241-269.

NEUMANN, E.-R. (1976): Compositional relations among pyroxenes, amphiboles and other mafic phases in the Oslo region plutonic rocks. *Lithos* **9**, 85-109.

PARSONS, I. (1979): The Klokken gabbro–syenite complex, south Greenland: cryptic variation and origin of inversely graded layering. *J. Petrology* **20**, 653-694.

PHILPOTTS, A.R. (1967): Origin of certain iron–titanium oxide and apatite rocks. *Econ. Geol.* **62**, 303-315.

POLDERVAART, A. & HESS, H.H. (1951): Pyroxenes in the crystallization of basaltic magma. *J. Geol.* **59**, 472-489.

POTAP'YEV, V.V. (1964): Decrease in the index of refraction of biotite in late-phase granite of the Kolyan massif (Altai). *Akad. Nauk SSSR, Dokl.* **155(3)**, 583-585.

TAYLOR, R.P. (1979): Topsails igneous complex–further evidence of Middle Paleozoic epeirogeny and anorogenic magmatism in the northern Appalachians. *Geology* **7**, 488-490.

TYLER, R.C. & KING, B.C. (1967): The pyroxenes of alkaline igneous complexes of eastern Uganda. *Mineral. Mag.* **36**, 5-21.

Received April 14, 1982, revised manuscript accepted October 4, 1982.